# Synthesis and Properties of Photosensitive Glycomacrocycles

**Juan Xie***

**DOI: 10.1039/b000000x [DO NOT ALTER/DELETE THIS TEXT]**

This review paper summarizes all fluorescent and photochromic glycomacrocycles reported to date. The synthetic strategies, their photophysical, photochemical, chiroptical and circularly polarized luminescence properties, as well as their applications from fluorescent ion sensing, DNA intercalation, to multistimuli-responsive organogels formation or as photoresponsive chiral dopants for cholesteric liquid crystals will be presented.

## 1 Introduction

The field of advanced photosensitive molecular systems is extremely active and has attracting ever-growing interest in recent years in many research areas for their potential applications in chemistry, biology, high-resolution imaging, molecular machines and optoelectronics.[1-9] Light can be easily and precisely controlled in time, location, wavelength and intensity, thus enabling the precise activation, deactivation, detection or modulation of various chemical and biological events. It is generally non-invasive and orthogonal toward most elements of living systems, offering the potential to interrogate biological processes by targeting very diverse analytes (from small ions to large macromolecules) or to change the properties of defined molecules with minimal disturbance to the rest of the biological system. Fluorescent compounds have proven to be particularly useful in biological, analytical as well as material sciences, with distinct advantages in sensitivity and biological imaging.[1-3] Photochromic molecules are bistable molecules featuring different structural and/or electronic properties which may be reversibly isomerized by light. Photoresponsive “intelligent” molecular systems based on photochromic molecules have been shown to be extremely promising for spatial and temporal control over various chemical and biological processes.[4-9]

Carbohydrate-based macrocyclic compounds have been developed for chemical, supramolecular, analytical and biological applications, or as biomaterials.[10] Development of photosensitive glycomacrocycles should be of particular interest for spatiotemporally controlling various chemical and biological properties of these compounds by light. The aim of this review is to provide an overview of all reported fluorescent and photochromic glycomacrocycles.

## 2 Fluorescent glycomacrocycles

Up to date, anthracene, pyrene, BODIPY and heterocyclic fluorophores have been introduced through ester, amide, ether or triazole linkage into the furanoside 1,5-position or the pyranoside 1,6-, 2,3- or 2,6-position to synthesize 10- to 28-membered fluorescent glycomacrocycles (Figure 1). Ion sensing, DNA binding, chiroptical and circularly polarized luminescence properties have been investigated.

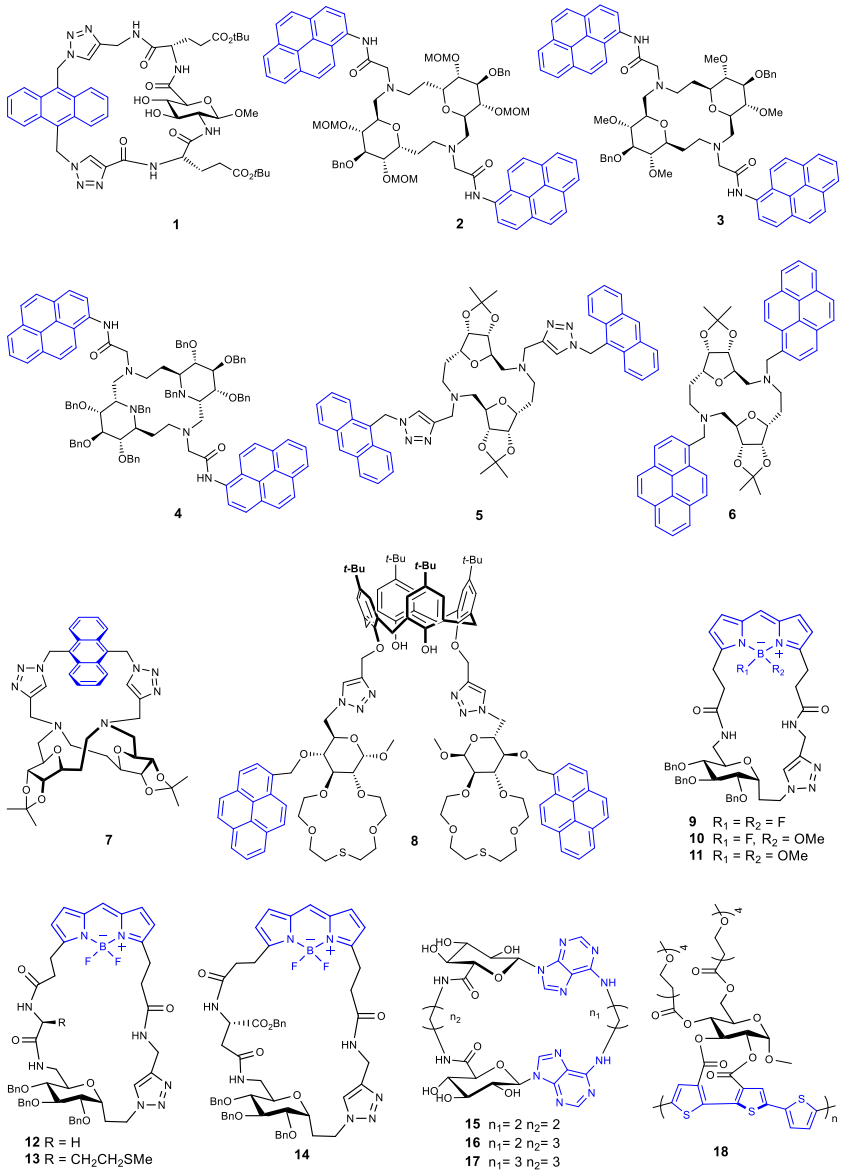


**Figure 1** Structure of reported fluorescent glycomacrocycles.

## 2.1 Synthesis

To the best of our knowledge, the first fluorescent glycomacrocycle has been reported by Nillson and co-workers in 2006.[11] The 9,10-bis(azidomethyl) anthracene **24** has been used to realize the macrocyclization through the Cu(I)-catalyzed azido-alkyne cycloaddition reaction (CuAAC) with the bis-alkyne-functionalized glycosylpeptide **23**, leading to the 27-membered glycomacrocycle **1** linked on the 2,6-position of sugar (Scheme 1). Compound **23** was prepared in three steps from the sugar aminoacid **19** and the alkyne-functionalized aminoacids **20** and **22**.

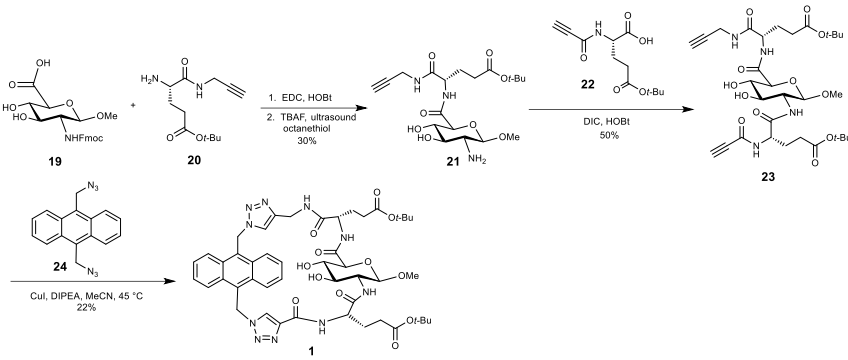


**Scheme 1** Synthesis of glycomacrocycle **1**.

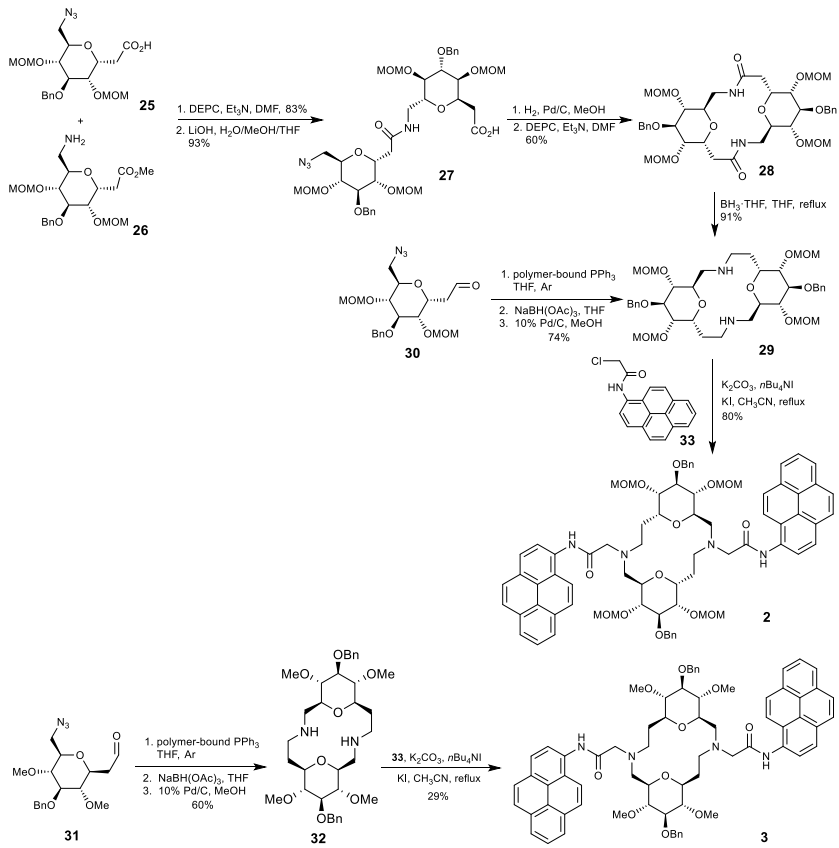


**Scheme 2** Synthesis of glycomacrocycles **2** and **3**.

The group of Xie has developed the fluorescent sugar-aza-crown (SAC) ethers **2** and **3** by introducing pyrene fluorophore on two nitrogen atoms of aza-crown ethers (Scheme 2).[12] The SAC ethers can be prepared either through reduction of amide-linked glycomacrocycle **28** with $BH_3$,[13] or through a one-pot cyclodimerization of *C*-

glycosyl azido aldehydes **30** or **31** via a domino Staudinger aza-Wittig reaction, followed by reduction of cyclic imine with $NaBH(OAc)_3$ and cleavage of borane-amine adducts with Pd/C.[14] *N*-alkylation with *N*-(1-pyrenyl)chloroacetamide **33** under basic condition led to the 14-membered glycomacrocycles **2** and **3** bearing different anomeric configurations.[12] These two macrocycles are constructed through the 1,6-position of *C*-glucoside derivatives.

Very recently, a pyrene-functionalized iminosugar azacrown ether has been reported by Blériot and colleagues[15] The 14-membered iminosugar azacrown ether **35** was prepared from the iminosugar aldehyde **34** by using a domino Staudinger aza-Wittig reaction followed by reduction of cyclic imine with $NaBH(OAc)_3$, method developed by Xie's group (Scheme 3).[14,16] *N*-alkylation with **33** then furnished the fluorescent glycomacrocycle **4**.[15]

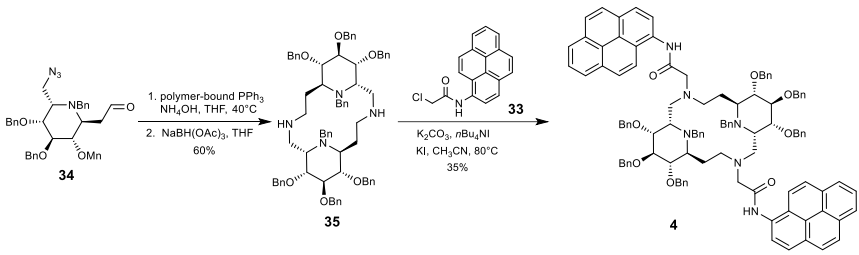


**Scheme 3** Synthesis of glycomacrocycle **4**.

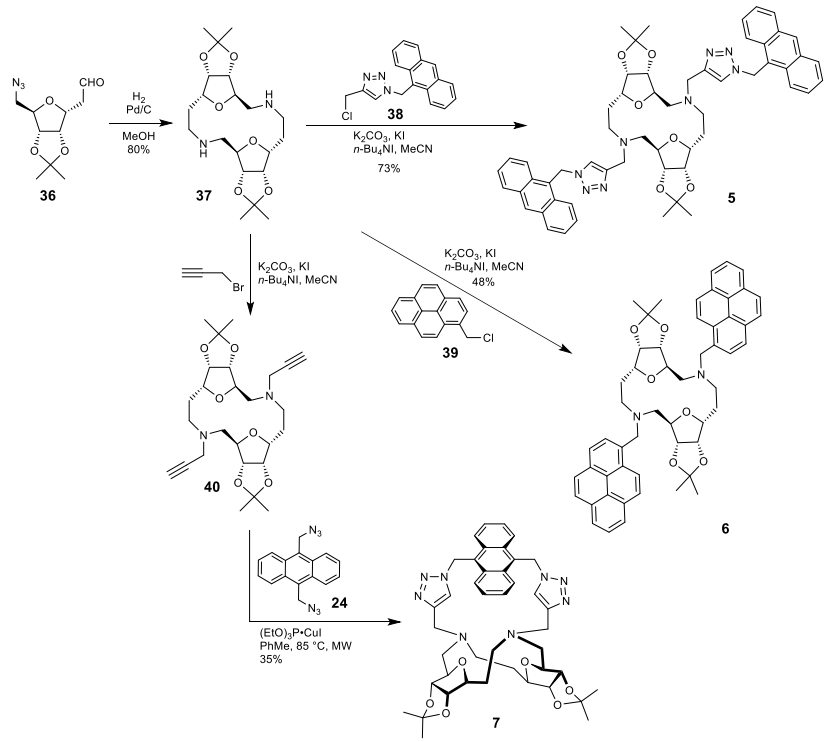


**Scheme 4** Synthesis of glycomacrocycles **5** to **7**.

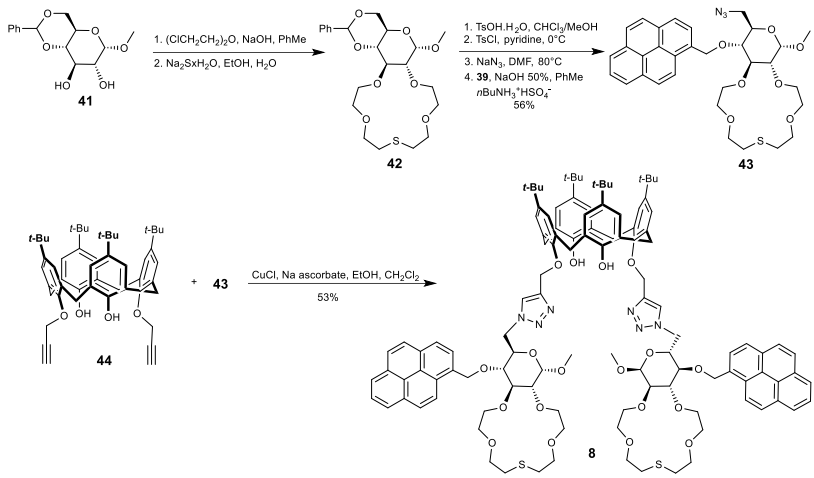


**Scheme 5** Synthesis of glycomacrocycle **8**.

Wu's group then developed anthracene or pyrene-functionalized furanoid SAC ethers **5**-**7**.[17-19] The SAC ether **37** was firstly synthesized through a one-pot cyclodimerization of *C*-ribosyl azido aldehyde **36** under hydrogenation conditions (Scheme 4).[20] This 14-membered glycomacrocycle **37** was built through the 1,5-position of the ribose derivative. *N*-alkylation with triazoyl anthracene **38** gave the glycomacrocycle **5**,[17] while the reaction with 1-chloromethylpyrene **39** furnished the glycomacrocycle **6**.[18] They have also prepared an anthracene-functionalized cavitand **7** through CuAAC of alkynylated SAC **40** with azidomethylanthracene **24**.[19]

A pyrene-functionalized sugar thiacrown ether appended calix[4]arene was reported by Ling *et al*.[21] The 15-membered sugar thiacrown ether **42** was prepared through 2,3-bis-*O*-alkylation of glucoside **41**, followed by macrocyclization in the presence of $Na_2S$ (Scheme 5). After introducing the pyrenylmethyl group on the 4-position, the azido compound **43** was then appended to the *O*-propargyl calix[4]arene **44** through CuAAC, leading to the desired compound **8**.

BODIPY-functionalized glycomacrocycles **9** to **14** have been synthesized by Xie's group from alkyne-functionalized BODIPY **49** and *C*-glucosyl azides by employing CuAAC for the macrocyclization step (Scheme 6).[22] After Boc-removal, the *C*-glucosyl azides **45**-**48** were coupled to the alkyne-BODIPY **49** affording compounds **50**-**53** which underwent intramolecular CuAAC to afford the corresponding glycomacrocycles **9**, **12**-**14**. The fluorescent $B(OMe)_2$ and BF(OMe) derivatives of BODIPY glycomacrocycles **10** and **11** can be readily prepared by treatment of **9** with $BCl_3$ in $CH_2Cl_2$ at -78 °C during 5 min. These 23 to 28-membered macrocycles are constructed through the 1,6-position of *C*-glucoside derivatives.

Cyclic glycosyl purines have been developed as DNA cyclointercalators by Jang's group.[23] These 26- to 28-membered glycomacrocycles **15**-**17** were synthesized from the glucuronosyl purine **54**, by reacting with ethanediamine or 1,3-propanediamine, followed by Zemplén deacetylation and transacylation by using ethanediamine or 1,3-propanediamine (Scheme 7).

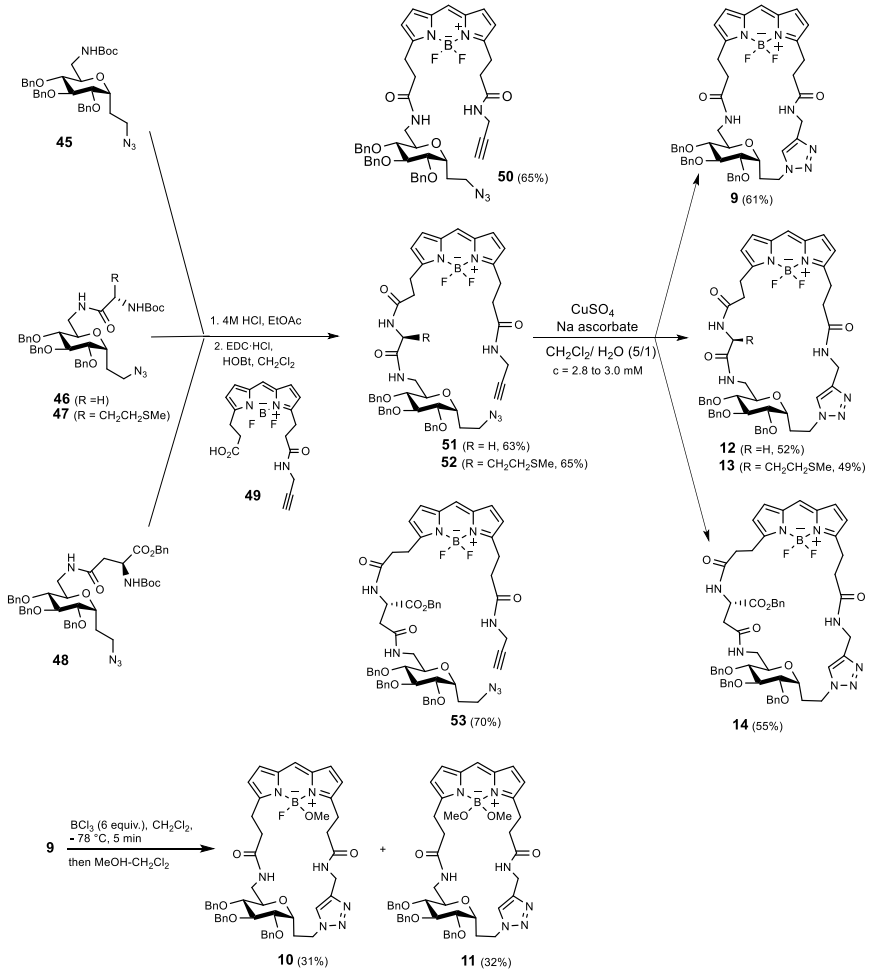


**Scheme 6** Synthesis of glycomacrocycles **9** to **14**.

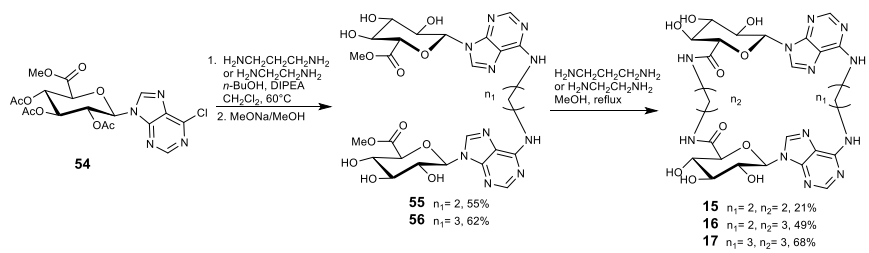


**Scheme 7** Synthesis of glycomacrocycles **15** to **17**.

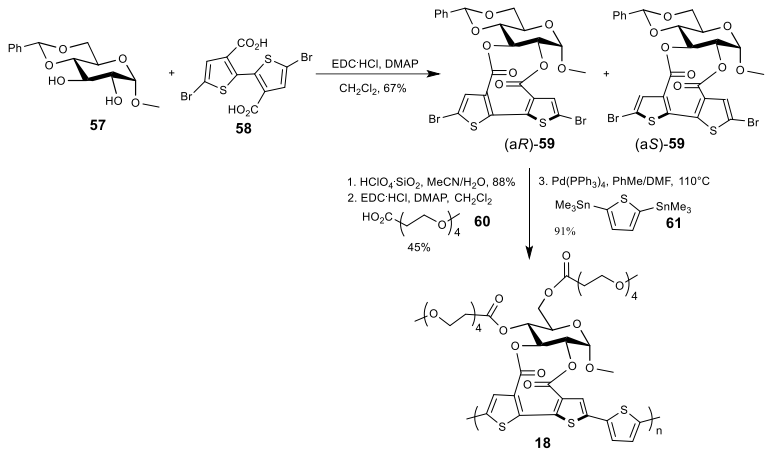


**Scheme 8** Synthesis of glycomacrocycle **18**.

Very recently, Ikai *et al.* have developed a one-handed sugar-based helical polythiophene.[24] Esterification of 4,6-*O*-benzylidene glucoside **57** with bithiophene derivative **58** led to 10-membered glycomacrocycle **59** as a mixture of a*R* and a*S* isomers, separable by HPLC (Scheme 8).[24,25] After benzylidene removal and esterification with **60** on the 4,6-position of glucoside, copolymerization of (a*R*)-**59** with 2-(tributylstannyl)thiophene **61** by Stille cross-coupling furnished the polymeric compound **18** with axial chirality. The molecular mass was estimated to be greater than 5600 g.mol$^{-1}$.[24]

## 2.2 Properties

### 2.2.1 Fluorescent chemosensors

Fluorescent glycomacrocycles including sugar (azaimino)(thia)crown ether derivatives and BODIPY-embedded macrocycles have demonstrated interesting fluorescent chemosensors properties.

The pyrene-functionalized SACs **2** and **3** displayed fluorescence characteristics of pyrene monomer ($\lambda_{max}$ = 385 nm) and intramolecular excimer emission due to strong $\pi$-$\pi$ interaction between two pyrenyl units ($\lambda_{max}$ ~ 480 nm) (Figure 2 and Figure 3 for the macrocycles **2** and **3**, respectively).[12] The excimer emission of **2** is weaker than **3**, probably due to different conformations adopted by these two compounds with different anomeric configurations. Ion recognition investigation by following fluorescence changes upon addition of 100 equivalents of divalent cations to the methanol solution of **2** or **3** showed that the total fluorescence intensity was not significantly affected by a representative selection of alkaline earth metal ions ($Mg^{2+}$, $Ca^{2+}$) and transition metal ions ($Co^{2+}$, $Mn^{2+}$, $Ni^{2+}$), but strongly quenched by $Cu^{2+}$ and $Cd^{2+}$ and to a less extent by $Pb^{2+}$ and $Zn^{2+}$. The titration experiment demonstrated the progressive fluorescent quenching upon increasing concentration of $Cu^{2+}$ (Figures 2 and 3, with the insets showing the decrease of fluorescence intensity as a function of $Cu^{2+}$ concentration). The curves were well-fitted with a 1:1 complexation equation model and provided high stability constants as followed: log *K*($Cu^{2+}$:**2**) = 6.7±0.2 and log *K*($Cu^{2+}$:**3**) = 7.8±0.3, with the detection limit of

$Cu^{2+}$ of 40 nM (2.5 µg.$L^{-1}$) for both compounds. Moreover, $Cu^{2+}$ concentration could be detected through a ratiometric measurement of the excimer-to-monomer ratio, as demonstrated by the decrease of the $I_{Exc}/I_{Mon}$ ratio of **3** while increasing the $Cu^{2+}$ concentration in Figure 3b. The molecular geometry optimization by DFT showed that the two pyrenyl substituents in **2** and **3** are free to adopt many accessible conformations and to form excimers, while $Cu^{2+}$-complexation rigidified the conformation and placing the pyrene moieties far apart (Figure 4). Consequently, excimer formation is conformationally prohibited in the complexes, which illustrated the complete quenching of the excimer emission. The $Cu^{2+}$ cation is shown to be coordinated with the two carbonyl groups and the two amino groups of SAC **2** with α-anomeric configuration, while two additional oxygen atoms from the SAC are involved into the coordination sphere in SAC **3** with β-anomeric structure which can explain the higher stability constant of the complex. It has to be noticed that the corresponding non fluorescent SACs **29** and **32** displayed also selective recognition towards $Cu^{2+}$ as revealed by mass spectrometry, and a better affinity to the β-anomer **32**.[26]

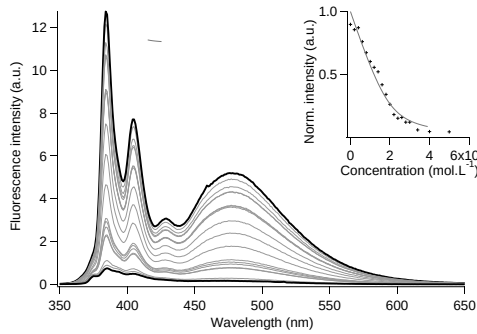


**Figure 2** Fluorescence spectra obtained during the titration of **2** in MeOH (2 µM) with $Cu(ClO_4)_2$ (from 0 to 2.5 eq.). $\lambda_{ex}$ = 340 nm. Inset: titration curve of the normalized integrated fluorescence as a function of $Cu^{2+}$ concentration. Reproduced from Ref. 12 with permission from American Chemical Society.

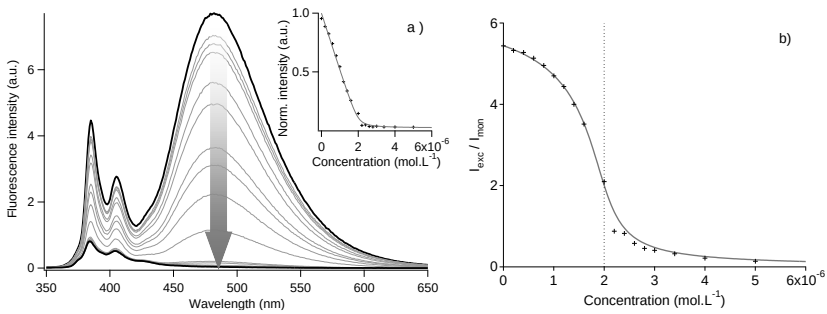


**Figure 3** (a) Fluorescence spectra obtained during the titration of **3** in MeOH (2 µM) with $Cu(ClO_4)_2$ (from 0 to 2.5 eq.). $\lambda_{ex}$ = 340 nm. Inset: titration curve of the normalized integrated fluorescence as a function of $Cu^{2+}$ concentration. (b) Relative intensity of the excimer and monomer emission bands ($I_{Exc}/I_{Mon}$) as a function of $Cu^{2+}$ concentration. Reproduced from Ref. 12 with permission from American Chemical Society.

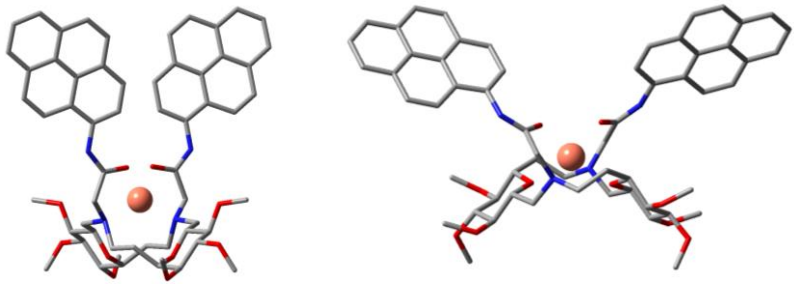

**Figure 4** B3LYP/6-31G energy-minimized structures of the $Cu^{2+}$-complexed SACs **2** (left) and **3** (right) by DFT calculations (To simplify the calculation, methyl ethers were used as hydroxy protecting groups). The LANL2DZ (ECP) basis set was used for the $Cu^{2+}$ cation. Reproduced from Ref. 12 with permission from American Chemical Society.

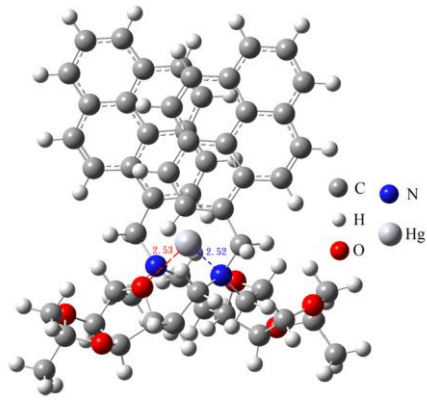


**Figure 5** Optimized conformation of $Hg^{2+}$-**6** complex by B3LYP/LanL2DZ. Reproduced from Ref. 18 with permission from Elsevier.

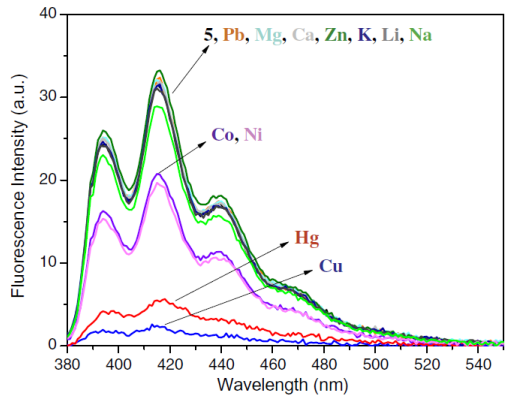


**Figure 6** Fluorescence spectra of **5** upon addition of $ClO_4^-$ salts of $Li^+$, $Na^+$, $K^+$, $Ca^{2+}$, $Mg^{2+}$, $Hg^{2+}$, $Co^{2+}$, $Ni^{2+}$, $Zn^{2+}$, $Cu^{2+}$ and $Pb^{2+}$ (100 eq.) in MeOH. $\lambda_{ex}$ = 367 nm. Reproduced from Ref. 17 with permission from Elsevier.

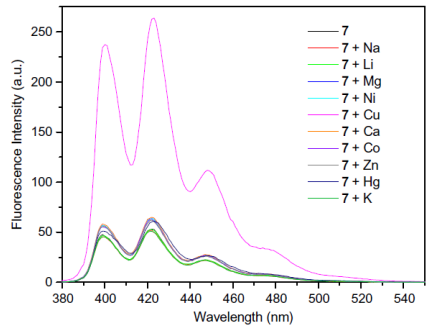


**Figure 7** Fluorescence spectra of **7** upon addition of $ClO_4^-$ salts of $Li^+$, $Na^+$, $K^+$, $Ca^{2+}$, $Mg^{2+}$, $Hg^{2+}$, $Co^{2+}$, $Ni^{2+}$, $Zn^{2+}$ and $Cu^{2+}$ (100 eq.) in MeOH. $\lambda_{ex}$ = 367 nm. Reproduced from Ref. 19 with permission from Elsevier.

Interestingly, the analogous sugar azaimino crown ether **4** exhibited a significant selective fluorescence quenching of the pyrene eximer in the presence of $Hg^{2+}$ ion, compared to other tested ions like $Cu^{2+}$, $Zn^{2+}$ and $Cd^{2+}$.[16]

For the furanoid SACs **5-7** (Figure 1), the pyrene-functionalized SAC **6** demonstrated high selective recognition toward $Cu^{2+}$ and $Hg^{2+}$ ions among a series of tested metal ions in methanol solution, with the association constants log $K$($Cu^{2+}$:**6**) = 1.9 and log $K$($Hg^{2+}$:**6**) = 3.6.[18] A 1:1 ligand-to-metal ratio was determined for the $Cu^{2+}$ or $Hg^{2+}$ion, and a detection limit of 130 μM for $Cu^{2+}$ and 12.6 μM for $Hg^{2+}$. The DFT-optimized conformation of the **6**-$Hg^{2+}$ complex showed that the $Hg^{2+}$ occupied the azacrown center and was closed to the two nitrogen atoms of the linker and two oxygen atoms of the ribosyl unit (Figure 5).

The anthracene-functionalized SAC **5** displayed three emission peaks around 395, 415, and 440 nm upon excitation at 367 nm.[17] As the macrocycle **6**, it also exhibited selective recognition of $Cu^{2+}$ and $Hg^{2+}$ ions among a series of tested metal ions (Figure 6). The calculated association constants were log $K$($Cu^{2+}$:**5**) = 5.6 and log $K$($Hg^{2+}$:**5**) = 5.0 in methanol, with the detection limits of 1.39 μM and 13.9 μM for $Cu^{2+}$ and $Hg^{2+}$ ions respectively.

The anthracene-functionalized cavitand **7** displayed similar emission spectrum as the macrocycle **5**, with maxima at approximately 402, 421, and 448 nm in methanol.[19] Interesting, fluorescence enhancement has been observed in the presence of $Cu^{2+}$ (Figure 7). The association constant for the determined 1:1 ligand metal ion complex has been calculated to be log $K$($Cu^{2+}$:**7**) = 4.4 in methanol.

As pyrene-functionalized SACs **2-4** and **6**, the pyrene-functionalized sugar thiacrown ether appended calix[4]arene **8** exhibited both monomer (378, 395 nm) and excimer (472 nm) emission bands when irradiated at 344 nm in methanol/chloroform.[21] Compound **8** exhibited selective fluorescence quenching in the presence of $Fe^{2+}$ and $Fe^{3+}$ ions, with the formation of 1:1 complexes and apparent association constants log $K$($Fe^{2+}$:**8**) = 2.95 and log $K$($Fe^{3+}$:**8**) = 2.94. Molecular mechanics energy optimization has been employed to determine the possible structure of the complexes (Figure 8). As for SACs **2** and **3**, iron complexation made the two pyrene moieties far apart, thus prohibiting excimer formation.

BODIPY-functionalized glycomacrocycles **9**, **12-14** displayed typical photophysical properties of BODIPY, with a maximum absorption band at 509 nm, and an emission band centered around 515 nm and a quantum yield up to 0.71 in acetonitrile (Figure 9).[22] The BF(OMe) and $B(OMe)_2$ derivatives **10** and **11**

displayed similar absorption and emission spectra as their $BF_2$ counterpart **9**, however with a higher quantum yield ($\Phi_F$ = 0.94) for the $B(OMe)_2$ BODIPY derivative **11**. The fluorescence emission of the macrocycles **9** and **12** can be selectively quenched by both cation ($Cu^{2+}$ and $Fe^{3+}$) and anions ($F^-$, $CN^-$) among tested cations and anions in acetonitrile. It has been determined that the glycomacrocycle **9** formed a 2:1 type complexes [$\mathbf{9}_2$·$Cu^{2+}$] and [$\mathbf{9}_2$·$Fe^{3+}$], with stability constants of $\log\beta_{21}$ = 13.6 and 11.2 for $Cu^{2+}$ and $Fe^{3+}$ respectively. Complexation study with non-cyclic precursors suggested the involvement of the triazole ring for $Cu^{2+}$ recognition, whereas $Fe^{3+}$ detection presumably occurs through the carbonyl groups. Investigation by $^{11}B$ and $^{19}F$ NMR spectroscopy revealed that $F^-$ and $CN^-$ quenched the BODIPY fluorescence through decomposition of the BODIPY core. Consequently, BODIPY derivatives behaved as chemodosimeters towards $F^-$ and $CN^-$.

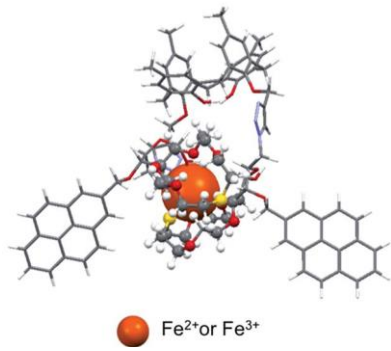


**Figure 8** Energy-minimized geometry of **8** binding $Fe^{2+}$ or $Fe^{3+}$. Reproduced from Ref. 21 with permission from The Royal Society of Chemistry.

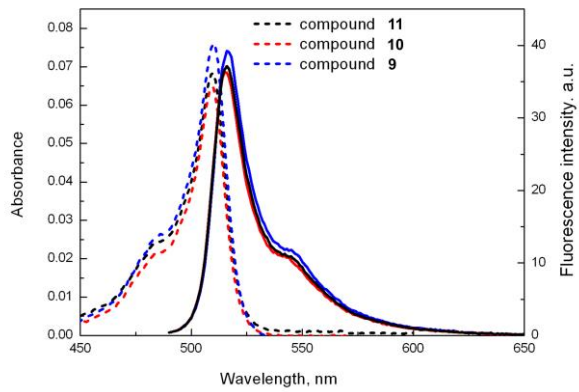


**Figure 9** Absorption (dotted lines) and fluorescence (full lines) spectra of compounds **9**-**11** in MeCN; [**9**] = [**10**] = [**11**] = 1 μM. $\lambda_{ex}$ = 508 nm. Adapted from Ref. 22 with permission from Wiley-VCH.

### 2.2.2 DNA intercalators

DNA intercalators are of particular interest for biological and pharmaceutical

applications. Based on docking simulations, Jiang *et al.* have developed three short linker-bridged cyclointercalators containing purine-glucuronic acid hybrids **15-17**.[23] Compounds **15-17** exhibited fluorescent emission bands near 385 and 495 nm in pH 7.4 phosphate buffer, when excited at 226 nm. The fluorescence intensity of **15-17** decreased with increasing concentration of calf-thymus DNA, with a more significant change for 27- and 28-membered macrocycles **16** and **17** compared to 26-membered macrocycle **15**. The intercalation with DNA has been further confirmed by a quenching assay based on the displacement of the known DNA intercalating ethidium bromide (EB), with a decrease of the fluorescence intensity of EB bound to DNA at 586 nm upon increasing concentration of **15-17**. The fluorescence quenching assay of EB bound to DNA showed that the cyclic compounds **15-17** exhibited similar affinity to DNA. However, their affinity is 1.4-2.9 times higher than the corresponding noncyclic precursors **55** and **56** (Scheme 7). Docking simulation demonstrated the binding geometries of **15-17** and the important role of the sugar moiety in the process of binding between the intercalators containing glucuronic acid and DNA (Figure 10). For the macrocycle **15 c**ontaining the shortest linker, it was unable to insert into the base pair stack, however able to bind to DNA thanks to several H-bonds between the sugar moiety and DNA. H-bonding between the sugar and DNA were also observed in 27- and 28-membered glycomacrocycles **16** and **17** which were able to interact with DNA as mono-intercalators.

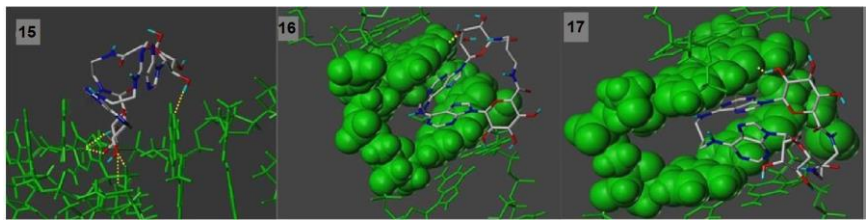


**Figure 10** Docking models of **15-17** (ball-and-stick representation colored in gray white). The DNA (PDB ID: 2ADW) was shown in green. Adapted from Ref. 23 with permission from Elsevier.

### 2.2.3 Chiroptical and circularly polarized luminescence properties

Thanks to their excellent semiconducting, optical and magnetic features, polythiophenes are an important class of π-conjugated polymers which have been widely studied for applications in organic devices and functional materials. Ikai *et al.* have developed chiral polythiophenes with macromolecular helicity.[24] The one-handed helical polythiophene **18** possessed a fixed *syn*-conformation of a D-glucose-linked bithiophene unit with a*R*-chirality. The circular dichroism (CD) spectra showed that poly-T$_R$ **18** showed a clear bisignated Cotton effect in the absorption region of 400-580 nm, with its CD intensity much larger than those observed for (a*R*)-**59** and the corresponding model-T$_R$ (Figure 11), suggesting a specific secondary structure within a single polymer chain. The intense CD signals of **18** were also observed in various solvent systems, with the CD signals molecular mass-dependent, characteristic of one-handed macromolecular helicity. All-atom MD simulation in chloroform of a corresponding model polythiophene demonstrated a left-handed helically folded conformation, in which a single turn of the helix was composed of approximately 15 thiophene rings and all sulfur atoms were arranged inside the helical cavity (Figure 11). Poly-T$_R$ **18** exhibited an apparent orange

photoluminescence (PL) in chloroform and in solid state under 365 nm irradiation (Figure 12). Furthermore, poly-$T_R$ **18** emitted right-handed circularly polarized light (CPL), with the maximum luminescence dissymmetry factor $|g_{lum}|$ values estimated to be $1.6 \times 10^{-3}$ in chloroform and $1.6 \times 10^{-3}$ in the film state (Figure 13).

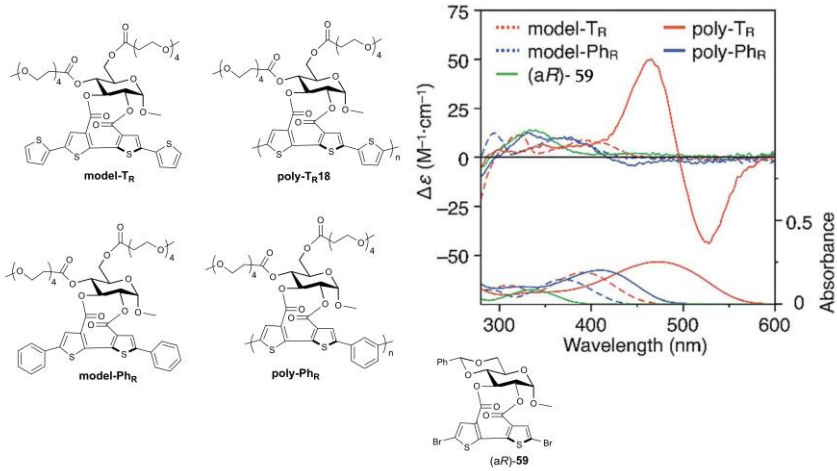


**Figure 11** Structure, CD and absorption spectra of polythiophenes in chloroform at 25 °C. [Glucose unit] = 0.1 mM. Adapted from Ref. 24 with permission from The Royal Society of Chemistry.

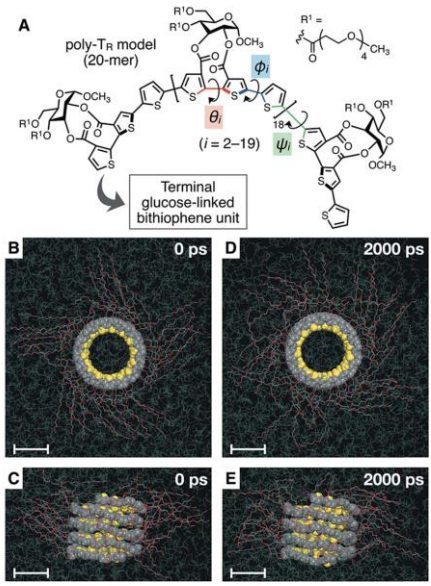


**Figure 12** (A) Structure of the poly-$T_R$ model used for the computational study. (B, D) Top view and (C, E) side view of the molecular model of left-handed helically folded poly-$T_R$ in chloroform at (B, C) 0 ps and (D, E) 2000 ps in an all-atom MD simulation after equilibration at 298 K, represented by space-filling (polythiophene backbone) and stick (side chain) models. All scale bars represent 1 nm. Reproduced from Ref. 24 with permission from The Royal Society of Chemistry.

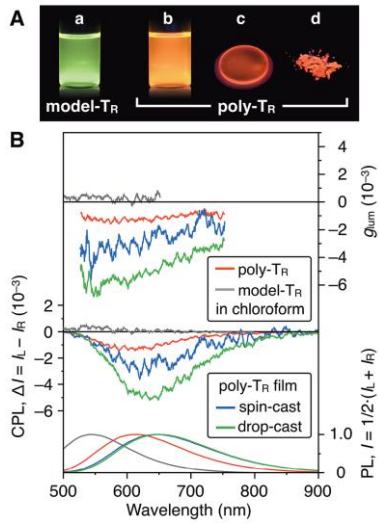


**Figure 13** (A) Photograph of chloroform solutions of (a) model-$T_R$ and (b) poly-$T_R$, and (c) the drop-cast film and (d) powder of poly-$T_R$ under irradiation at 365 nm. (B) PL (bottom), CPL (middle) and glum (top) spectra of poly-$T_R$ and model-$T_R$ in chloroform ([Glucose unit] = 0.1 mM) and the poly-$T_R$ films at room temperature. $\lambda_{ex}$ = 365 nm. Reproduced from Ref. 24 with permission from The Royal Society of Chemistry.

## 3 Photochromic glycomacrocycles

Photochromic compounds are attracting more and more research interest for various applications in organic chemistry, photochemistry, photophysics, supramolecular chemistry as well as material sciences. Molecular photoswitches allow reversibly photomodulating the conformation, shape, polarity and solubility of molecules, but also remote-controlling chemical reactivity or catalytic activities, biological and pharmacological properties.[4-9] The photochromic glycomacrocycles have been reported since 2017.[27-32] Up to date, among different molecular photoswitches such as diarylethene, azobenzene, spiropyrane, (hemi)(thio)indigos, acylhydrazone etc, only *o*- and *p*-dihydroxyazobenzenes have been introduced into the glycomacrocycles (Figure 14). Azobenzenes are T-type photochrome, meaning that isomerization between *E* (*trans*) and *Z* (*cis*) isomers can be stimulated by light and temperature, with the *E*-azobenzene usually more stable than the Z-isomer.[33] The dihydroxyazobenzene has been connected either to the anomeric or to the 6-position (with or without linker) of mono- or disaccharides for the glycomacrocycles **62**-**64** and **69**-**75** containing two or four sugar units, and to the 2,3 or 4,6-position of glycopyranosides (**65**-**68**), furnishing 16- to 38-membered macrocycles.

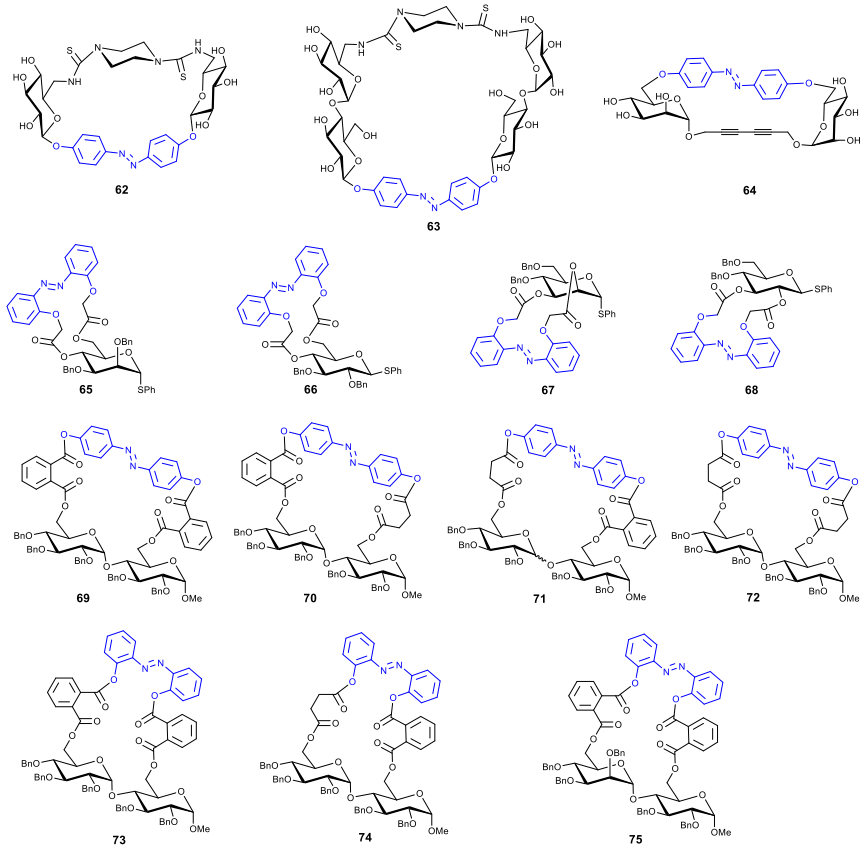


**Figure 14** Structure of reported photochromic glycomacrocycles.

### 3.1 Glycomacrocycles with azobenzene linked to the anomeric position

Despras *et al.* have first reported the azobenzene-functionalized glycomacrocycles **62** and **63**.[27] The *p*-dihydroxyazobenene **78** was linked to the anomeric position of glucose or maltose derivative through the imidate glycosylation method (Scheme 9). The azide functions were then converted into the corresponding isothiocyanates **79** and **80**. However, the macrocyclization with piperazine gave only trace amount of the macrocycles **81** and **82**. Interestingly, photoisomerization of compounds **79** and **80** into their *Z*-isomers followed by reaction with piperazine led to the desired acetylated macrocycles *Z*-**81** and *Z*-**82** which then underwent the thermal return to the more stable *E*-macrocycles. Zemplén deacetylation furnished the 28- and 38-membered macrocycles **62** and **63** respectively.

The absorption spectra of both *E*-isomers of **62** and **63** exhibited a large band with a maximum at around 350 nm, corresponding to the $\pi \rightarrow \pi^*$ transition of the azobenzene and a shoulder from 400 to 500 nm (an overlap between the $\pi \rightarrow \pi^*$ and $n \rightarrow \pi^*$ bands) (Figure 15a,b). The *E*-isomers can be easily isomerized to the *Z*-isomers upon irradiation at 365 nm with an excellent conversion (*Z*:*E* ratio of 98:2 for **62** and 96:4 for **63** in the photostationary state (PSS), as determined by $^1$H NMR)

(Figure 15). The *Z*-isomers showed a π→π* absorption band at around 310 nm and the n→π* band at around 440 nm. Irradiation at 435 nm converted partially the *Z*-isomers back to the *E*-isomers (*E*:*Z* ratio of 53:47 for **62** and 63:37 for **63** at $PSS_{435}$), because of spectral overlap of *E*- and *Z*-isomers. The photoisomerization can be repeated more than 10 times without any degradation, showing the high fatigue resistance. The *Z*-isomers can also be fully converted back into the *E*-isomers by heating in the dark for 16 h at 45°C. The half-life has been determined to be 6.2 h and 17.2 h in $D_2O$ at 27°C for *Z*-**62** and *Z*-**63** respectively. NMR spectroscopy has demonstrated that photoswitching induced a significant structural change, with a restricted conformational freedom in both *E* and *Z* states.

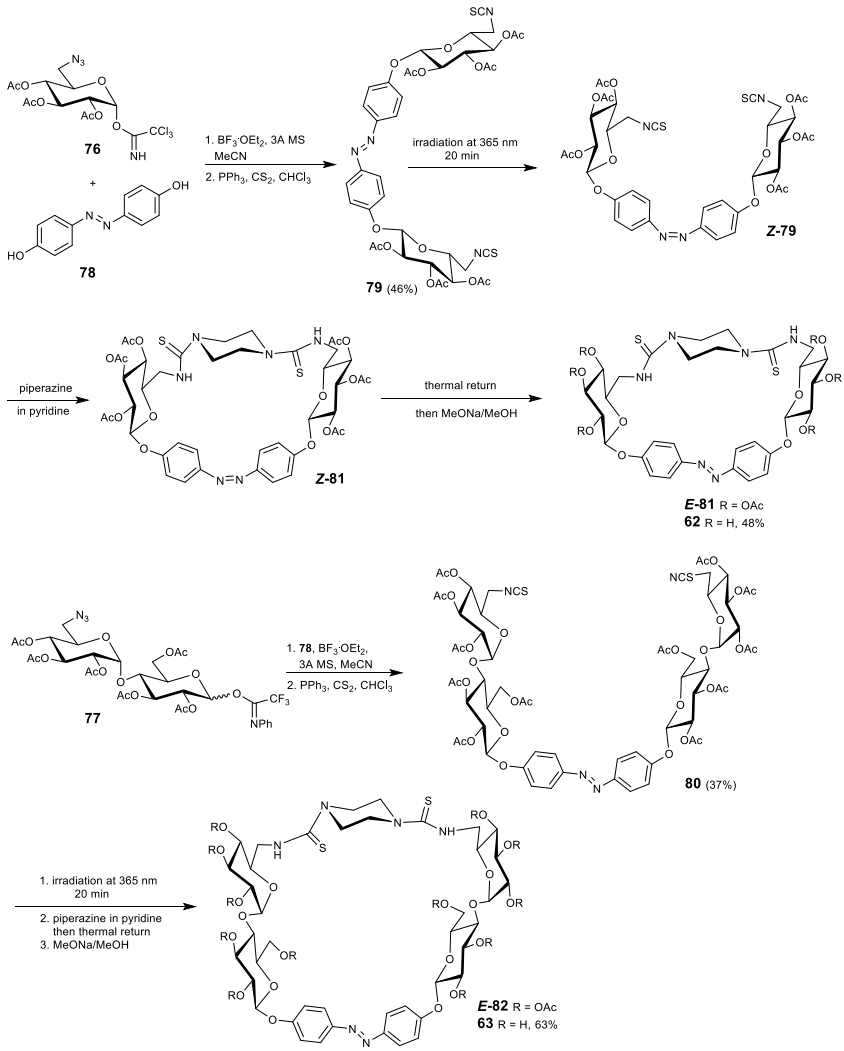


**Scheme 9** Synthesis of glycomacrocycles **62** and **63**.

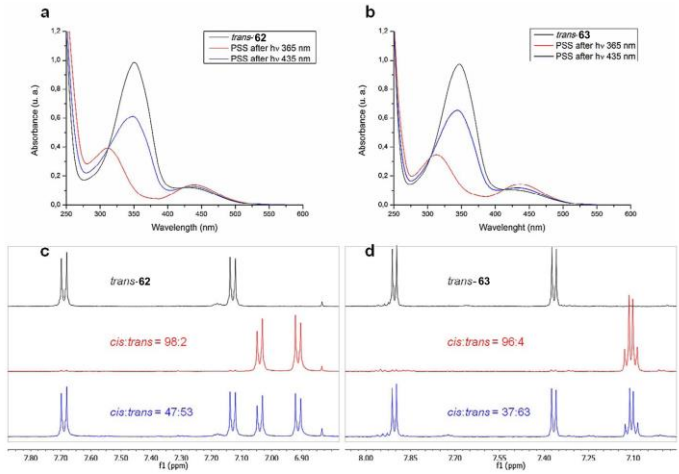


**Figure 15** Absorption spectra of **62** (50 μM in $H_2O$ (0.5% DMSO)) (a) and **63** (50 μM in $H_2O$) (b) at 298 K. Black line: *E*-isomers; red lines: PSS after irradiating the *E*-form at 365 nm; blue line: PSS after irradiating the *Z*-form at 435 nm; Partial $^1$H NMR spectra of **62** ($D_6$-DMSO) (c) and **63** ($D_2O$) at 300 K. (d) Black line: *E*-isomers; red line: PSS after irradiating the *E*-form at 365 nm; blue line: PSS after irradiating the *Z*-form at 435 nm. Adapted from Ref. 27 with permission from Wiley-VCH.

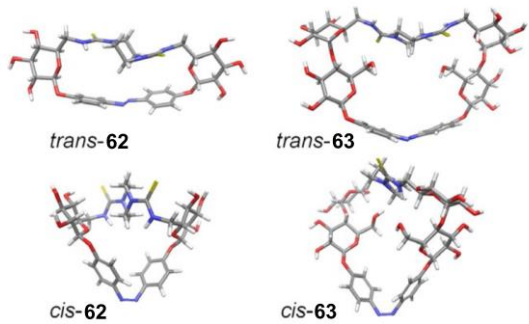


**Figure 16** Low-energy conformers of *trans* and *cis* forms of **62** and **63** calculated with Macromodel 11.1 (OPLS3 force field in implicit water). Adapted from Ref. 27 with permission from Wiley-VCH.

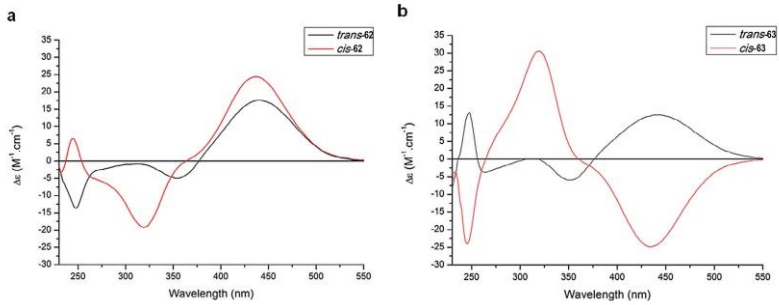


**Figure 17** Chiroptical properties of **62** and **63**. Circular dichroism spectra of **62** (50 μM in $H_2O$ (0.5% DMSO)) (a) and **63** (50 μM in $H_2O$) (b), before (black line, trans) and after (red line, PSS) irradiation at 365 nm. Adapted from Ref. 27 with permission from Wiley-VCH.

Stochastic dynamics with MacroModel has been performed to generate plausible conformation, demonstrating the significant shape modification after photoisomerization (Figure 16). Photoisomerization induced also significant change of specific rotation. Furthermore, the CD spectra showed chiroptical properties for both macrocycles, with a positive Cotton effect near 440 nm for the *E*-isomers (Figure 17). Interestingly, photoisomerization of *E*-**63** led to CD signals inversion, with a negative Cotton effect at 434 nm for *Z*-**63**.

### 3.2 Glycomacrocycles with azobenzene linked to a monosaccharide

Xie *et al.* have synthesized four glycomacrolactones with di-*o*-hydroxy azobenzene linked to 4,6 or 2,3-position of mannosides (**65**, **67**) and glucosides (**66**, **68**).[28,30] The glycomacrocycles have been prepared through the one-pot *O*-alkylation-mediated macrocyclization reaction between di-*O*-bromoacetyl thio-α- or β-D-glycopyranosides **83**-**86** and 2,2'-dihydroxyazobenzene **87** under basic conditions in the presence of crown-ether, affording 16- to 17-membered glycomacrocycles **65**-**68** in 22 to 39 % yield (Scheme 10).

As the macrocycles **62** and **63**, compounds **65**-**68** showed similar absorption spectra, with a relatively strong π→π* transition ($\lambda_{max}$ = 310-314 nm) and a weaker forbidden n→π* transition ($\lambda_{max}$ = 451-458 nm) of azobenzene moiety (see example for compound **65**: Figure 18). Irradiation at 365 nm resulted in the *E*→*Z* isomerization of the macrocycles. At $PSS_{365}$, *E*:*Z* ratio varied from 5:95 (for **65**), 10:90 (for **66**) and 15:85 (for **68**) to 20:80 (for **67**), with higher *E*→*Z* conversion for the 17-membered 4,6-*O*-linked macrocycles **65** and **66**. Back *Z*→*E* photoisomerization can be achieved by irradiation at 435 nm, with *E*:*Z* ratio varied from 53:47 to 70:30 at $PSS_{435}$. Interestingly, the macrocycles **65**-**68** exhibited higher thermal stability than other reported cyclic azobenzenes (with or without sugar moiety), with the *gluco* derivatives *Z*-**66** and *Z*-**68** (half-life at 293 K: 72 and 56 days respectively) more stable than the corresponding *manno* derivatives *Z*-**65** and *Z*-**67** (51 and 37 days respectively). Compounds **65**-**68** exhibited excellent fatigue resistance since photoswitching cycles have been repeated more than 15 times without any noticeable degradation. Chirality transfer from the sugar unit to azobenzene has also been observed for both *E*- and *Z*-glycomacrocycles **65**-**68**, with a negative band at around 454 nm and a positive band (310-350 nm) corresponding respectively to n→π* and π→π* transitions of the *E*-azobenzene in acetonitrile (Figure 19, black line), and a blue shift of all CD bands, without sign reversal for the *Z*-isomers ($PSS_{365}$, Figure 18, yellow line). DFT geometry optimization of different isomers of macrocycles followed by theoretical CD spectra calculation by TD-DFT suggest that the *E*- and *Z*-glycomacrocycles adopt preferentially (*P*) helical structure for the azobenzene moiety, after comparison with the experimental CD spectra (Figure 18).

Furthermore, among these four macrocycles, *manno*-macrolactone **65** exhibited gelation ability in cyclohexane and EtOH, with multistimuli-responsive behavior upon exposure to thermal-, photo-, and mechanical stimuli (Figure 19).[28] Moreover, the organogel in cyclohexane displayed a temperature-dependent helical inversion, with a positive Cotton effect at 460 nm which is inverted compared to its solution state which can be tuned by a repeated heating-cooling procedure (Figure 20). This could be a consequence of supramolecular chirality in the gel state.

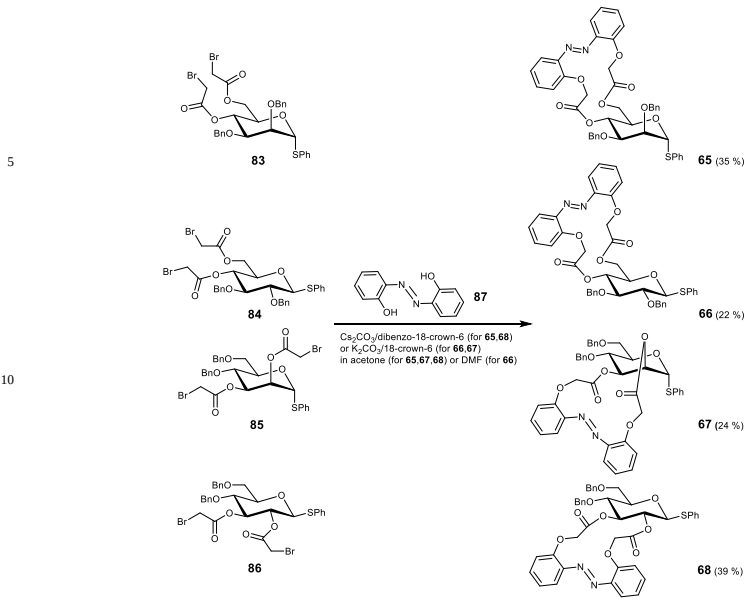


**Scheme 10** Synthesis of glycomacrocycles **65** to **68**.

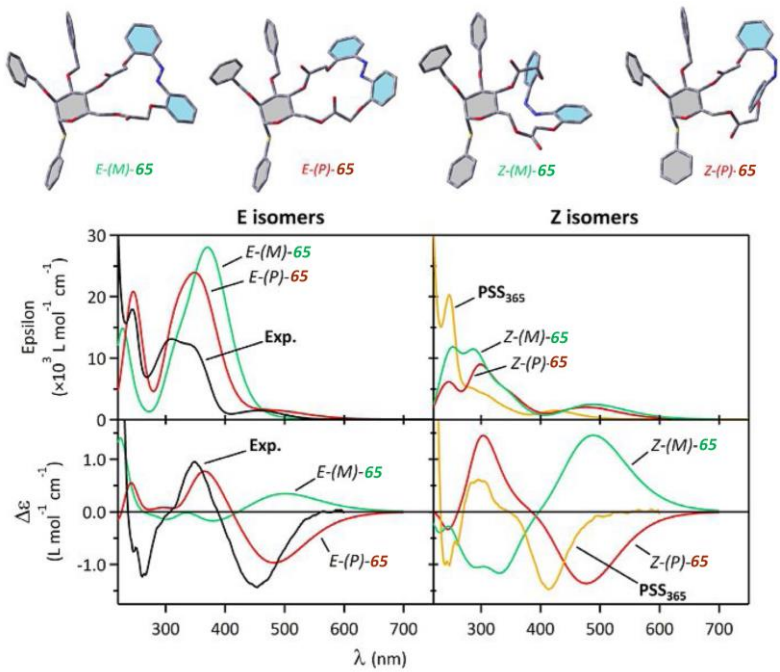


**Figure 18** Optimized structures of *E*-(*P*)-**65**, *E*-(*M*)-**65**, *Z*-(*P*)-**65** and *Z*-(*M*)-**65** by DFT at the B3LYP/6-311G level (top); and the calculated absorption (middle) and CD spectra (down) by TD-DFT calculations at the PBE0/6–311+G (d,p) level in acetonitrile. The calculated values have been divided by 25 times. The experimental spectra are also superimposed (black and yellow lines). Adapted from Ref. 28 with permission from Wiley-VCH.

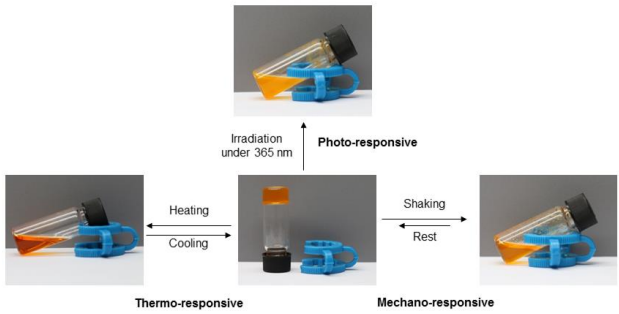


**Figure 19** Pictures demonstrating the multistimuli-responsive behavior of **65** gel in cyclohexane (3 mM). Reproduced from Ref. 28 with permission from Wiley-VCH.

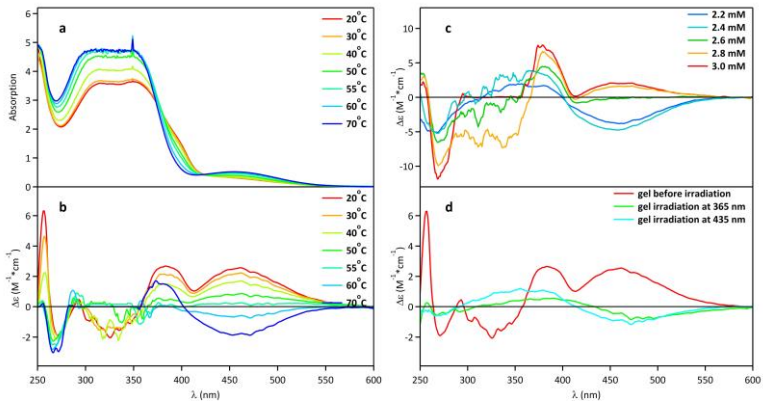


**Figure 20** a) Temperature-dependent absorption and b) CD spectra of **65** gel in cyclohexane (3 mM) (0.25 mm path length); c) Concentration-dependent CD spectra of **65** in cyclohexane at room temperature (1 mm path length); d) CD spectra of gel **65** before irradiation (red line), and after irradiation at 365 nm (48 $mWcm^{-2}$, 1 h) (green line) and at 435 nm (23 $mWcm^{-2}$, 1 h) (cyan line) (0.25 mm path length). Reproduced from Ref. 28 with permission from Wiley-VCH.

The glycomacrocycles **65** and **68** have also been investigated as photoresponsive chiral dopants for cholesteric liquid crystals (CLCs).[32] The resulting photoresponsive CLCs exhibited un unprecedented shortening of helical pitch length. The empowerment of helical twisting power (HTP) up to 500% was observed for **68** upon *E* to *Z* photoisomerization at 365 nm (Figure 21), reflecting the significant increase in the chirality transferability in the *Z*-azobenzene. It has to be noticed that larger HTP in the *Z*-rich state than that in the *E*-state is hardly attainable in common azobenzene dopants based CLC system. Rotational motion of a glass flake on the surface of the doped CLC mixture film has been achieved upon continuous UV/vis irradiation with both macrocycles **65** and **68**. With low intensity UV irradiation followed by visible irradiation at 510 nm, two-directional motion (clockwise and anticlockwise) occurred for **65** and **68** (Figures 22, 23), while one-directional rotational motion (crankshaft mode) is realized for **68**-doped CLC under full intensity UV light and visible irradiation (Figure 24). This phenomenon is of particular interest because this system meets the requirements to be considered as real molecular machinery which can continuously utilize the external light energy to perform mechanical work using the molecular switching mechanism.

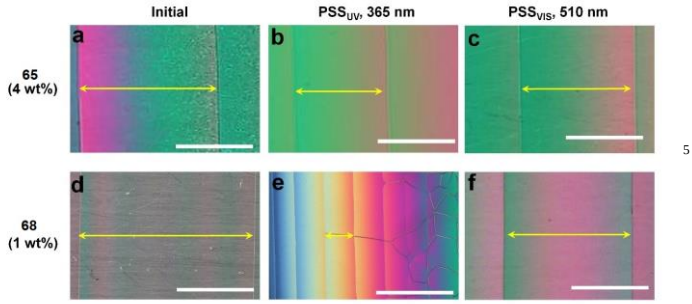


**Figure 21** Cano wedge cell images with Cano lines obtained from CLC mixtures containing 4 wt% of **65** in 5CB (a: initial, $P$ = 7.4 μm, b: $PSS_{UV}$, $P$ = 4.7 μm, c: $PSS_{vis}$, $P$ = 5.9 μm) and 1 wt% of **68** in ZLI-1132 (d: initial, $P$ = 8.4 μm, e: $PSS_{UV}$, $P$ = 1.4 μm, f: $PSS_{vis}$, $P$ = 5.9 μm). White scale bar: 100 μm. Adapted from Ref. 32 with permission from American Chemical Society.

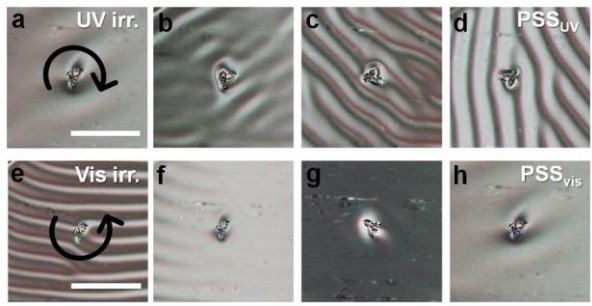


**Figure 22** Rotational motion of a glass flake on the surface of CLC mixture film (1.4 wt% of **65** in 5CB) upon continuous UV light irradiation of low intensity (2 $mWcm^{-2}$) from $PSS_{vis}$ (a) to $PSS_{UV}$ (d) in the clockwise direction. Counter-clockwise rotational motion from $PSS_{UV}$ (e) to $PSS_{vis}$ (h) upon visible light irradiation (25 $mWcm^{-2}$). White scale bar: 100 μm. Reproduced from Americain Chemical Society.

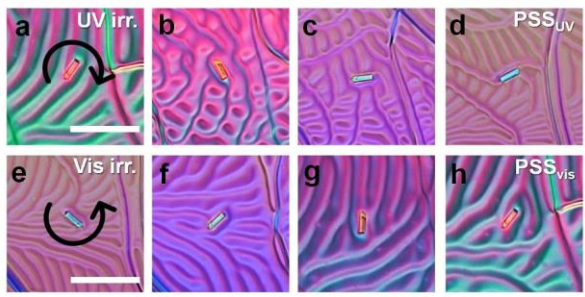


**Figure 23** Rotational motion of a glass rod on the surface of CLC mixture film (1 wt% of **68** in ZLI-1173) upon continuous UV light irradiation of low intensity (2 $mWcm^{-2}$) starting from $PSS_{vis}$ (a) to $PSS_{UV}$ (e) exhibiting 570º in the clockwise direction. Counter-clockwise rotational motion from $PSS_{UV}$ (e) to $PSS_{vis}$ (h) upon visible light irradiation (25 $mWcm^{-2}$) exhibiting 640º. White scale bar: 100 μm. Reproduced from Ref. 32 with permission from American Chemical Society.

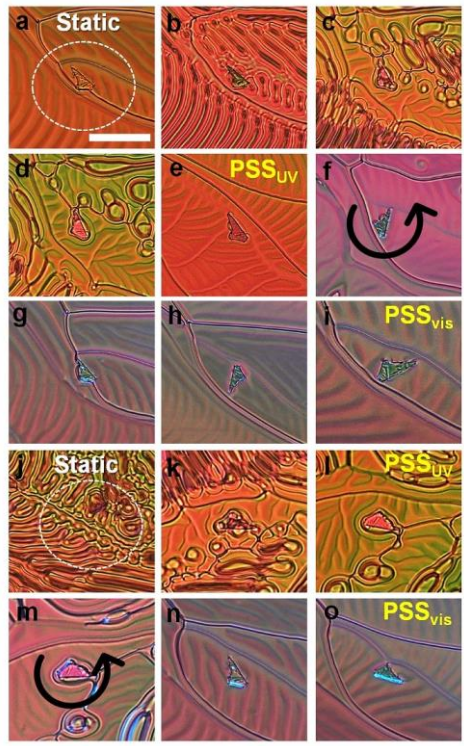


**Figure 24** Unidirectional rotational motion of a glass flack on the surface of CLC mixture film (1.7 wt% of **68** in 5CB) upon two rounds of alternating UV (full intensity, 8 $mWcm^{-2}$) and visible light (25 $mWcm^{-2}$) irradiation. It showed non-rotating static state upon the first (a→e) and the second (j→l) UV irradiating step. Counter-clockwise rotational motion was observed upon the first (f→i) and the second (m→o) visible light irradiating step exhibiting rotation angles of 310º and 340º, respectively. White scale bar: 100 μm. Reproduced from Ref. 32 with permission from American Chemical Society.

### 3.3 Glycomacrocycles with azobenzene linked to the 6-position of carbohydrate

Despras *et al.* have prepared the 28-membered glycomacrocycle **64** through Mitsunobu reaction between the *O*-propargyl mannoside **88** and *p*-dihydroxyazobenzene, followed by acetylation, Glaser coupling and Zemplén deacetylation (Scheme 11).[29] Once again, the macrocyclization was achieved with the *Z*-azobenzene **89**, the reaction concentration was shown to be important for the cyclization yield.

Compound **64** displayed excellent photoswitching ability and high fatigue resistance as other azobenzene-functionalized glycomacrocycles. Irradiation at 365 nm converted efficiently the *E*-macrocycle into the corresponding *Z*-isomer with a *Z*:*E* ratio of 98:2, and a significant shape change, as demonstrated by NMR study (Figure 25). Interestingly, the *Z*→*E* isomerization can be realized by irradiation with a green light, with a good *E*:*Z* ratio of 88:12 at $PSS_{525}$. The half-life of the *Z*-**64** was measured to be 114 h at 27°C in DMSO. Chiroptical properties have also been observed for both isomers in DMSO, with a negative CD signal at 360 nm and a weaker one at 440 nm for the *E*-isomer, and a positive band at 320 nm and a strong

negative band at 440 nm for the *Z*-isomer ($PSS_{365}$). Moreover, a solubility switch has been realized in water which was visible with the naked eye at higher concentrations, where the *E*-isomer is less soluble that the more polar *Z*-isomer (Figure 26). This solubility tuning is reversible under UV and green light irradiation.

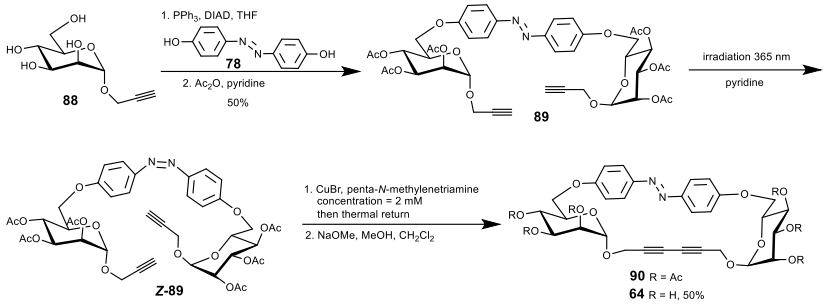


**Scheme 11** Synthesis of glycomacrocycle **64**.

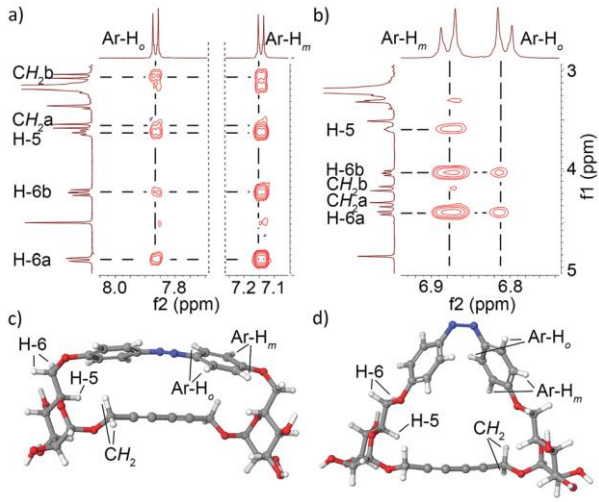


**Figure 25** (a) Expansion of the NOESY spectrum for *E*-**64** and (b) PSS at 365 nm in DMSO at 300 K; (c) force field-minimized structures of *E*-**64** and (d) *Z*-**64**. Reproduced from Ref. 29 with permission from The Royal Society of Chemistry.

**Figure 26** Reversible switching of the solubility: *E*-**64** in water (1.0 mg $mL^{-1}$) and after irradiation with 365 nm for 3 min and 525 nm for 10 min. Reproduced from Ref. 29 with permission from The Royal Society of Chemistry.

Xie's group has investigated an intramolecular glycosylation approach with a photochromic template and the influence of azobenzene configurations on the glycosylation outcome for the synthesis of photoswitchable glycomacrocycles (Figure 27).[31] Since the substrate conformation could influence the efficiency of the macrocyclization reaction, it was expected that the *E*→*Z* photoisomerization of azobenzene could induce a large change in conformation and the disposition between the glycosyl donor and glycosyl acceptor, and consequently influence the efficiency and the stereoselectivity of the macrocyclization by stereoelectronic and conformational effects. It has to be noticed that, for the synthesis of glycomacrocycles through thiourea formation (**62** and **63**, Scheme 9)[27] or Glaser coupling (**64**, Scheme 11),[29] only *Z*-azobenzene-linked substrates allowed the macrocyclization.

Glycosyl donor-acceptor compounds functionalized with *p*-/*o*-hydroxyazobenzene through a phthaloyl and/or succinoyl linkers (**102**-**108**, Scheme 12) can be readily prepared from the glucosides or mannoside, respectively, by successive coupling with phthaloyl or succinoyl anhydride and dihydroxyazobenzene. Intramolecular glycosylation of *E*-isomer of **102**-**108** activated by NIS/TfOH occurred with high α-selectivity except the macrocycle **71** (Schemes 12, 13). The 30-membered glycomacrocycles **69**-**75** were obtained in 12-60 % yield, with higher yields (45-60 %) for more rigid phthaloyl-linked compounds **69**, **73** and **75**. UV irradiation converted the *E*-substrates to the corresponding *Z*-**102**-**108** with a *Z*/*E* ratio from 78/22 to 89/11 at $PSS_{370}$. Intramolecular glycosylation of *Z*-isomers under same condition was also α-selective, however with lower yield (30% max.). In most of cases, *E*-macrocycles have also been isolated because of thermal return of the *Z*-macrocycles and/or the cyclization product from the *E*-substrate presented at PSS. This study showed that excellent α-stereoselectivity can be achieved by using *p*- and *o*-dihydroxyazobenzenes templates, demonstrating the proof-of-concept of using photoswitchable template to achieve the challenging 1,2-*cis* glycosylation.

The glycomacrocycles **69**-**75** can be reversibly photoisomerized between *E* and *Z* isomers under illumination at 370 nm and 433 nm, with high fatigue resistance. DFT calculations demonstrated that all the *E*-α-macrocycles are more stable than the *Z*-α-isomers, with the macrocycles bearing two phthaloyl linkers being more stable. The half-live for *Z*-**73** and *Z*-**74** has been estimated to be 299.3 h and 270.5 h respectively at 25°C in $CH_2Cl_2$. Also, among the linear and cyclic azobenzene derivatives, only the *o*-substituted cycloazobenzenes **74** and **75** exhibited chiroptical properties, with inversion of helical chirality upon *E*→*Z* photoisomerization for **74** (Figure 28).

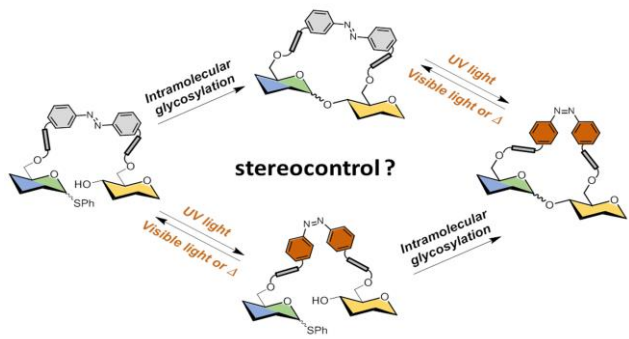

**Figure 27** Photoswitchable glycomacrocycles through intramolecular glycosylation approach. Adapted from Ref. 31 with permission from The Royal Society of Chemistry.

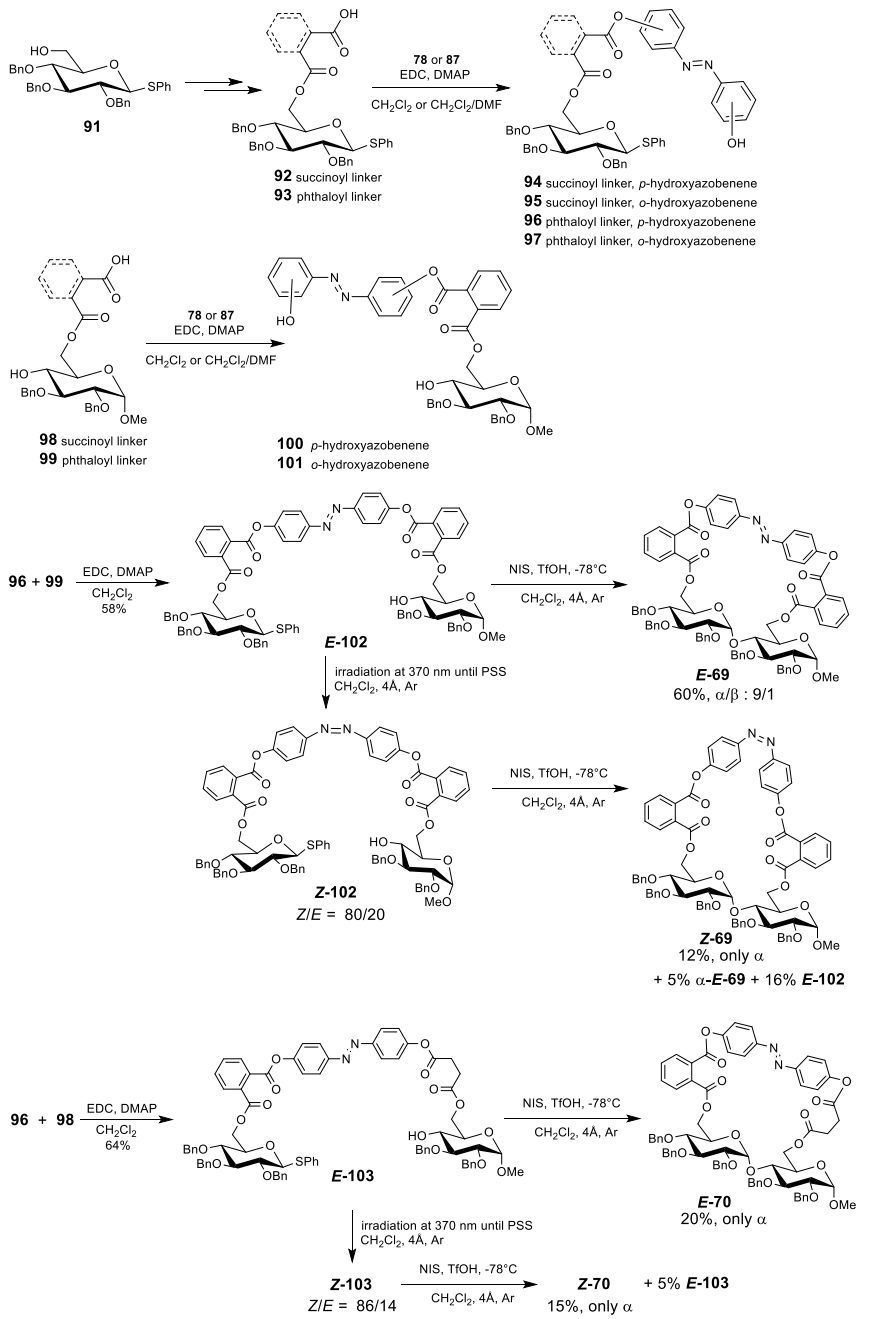


**Scheme 12** Synthesis of glycomacrocycles **69** and **70**.

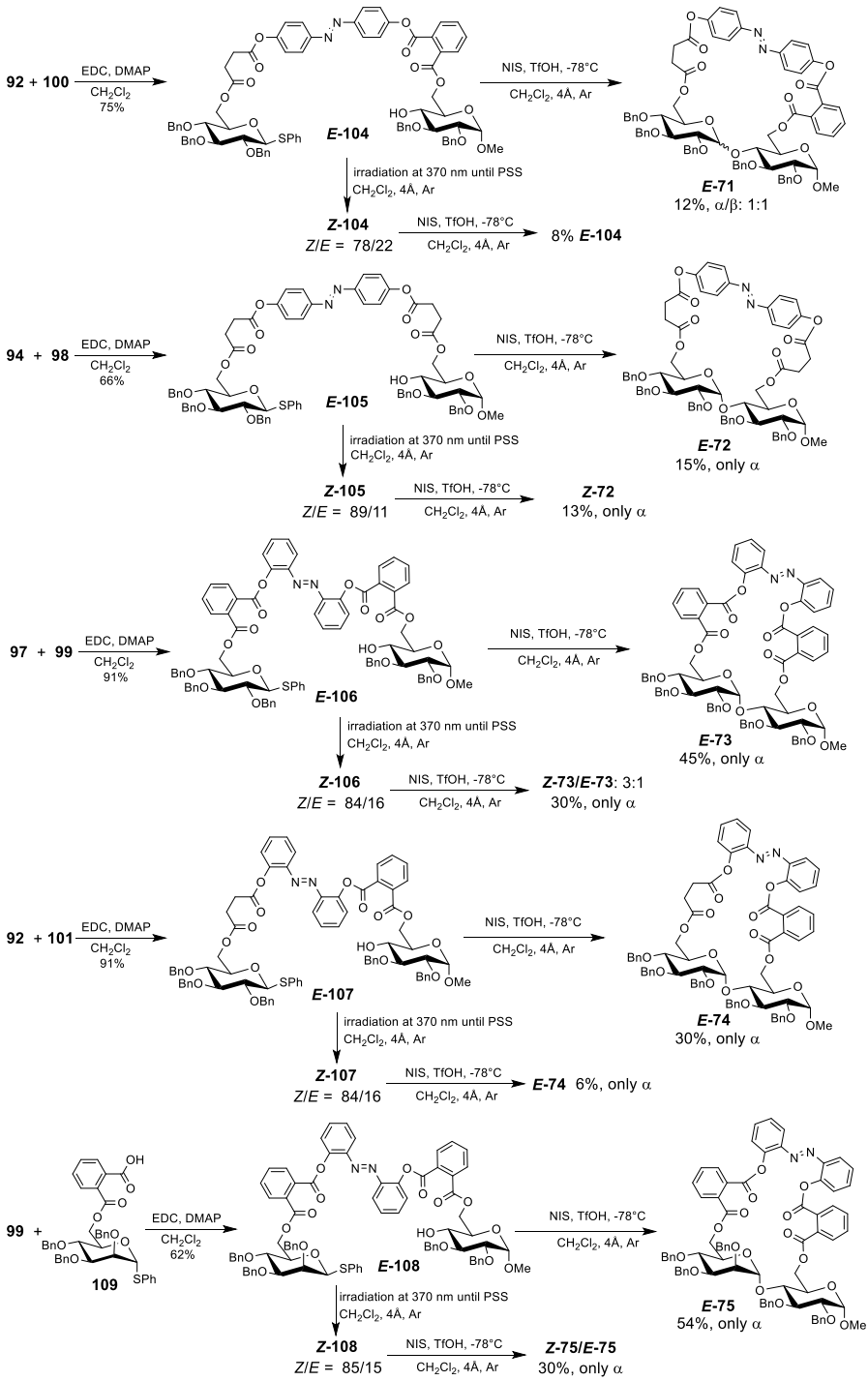


**Scheme 13** Synthesis of glycomacrocycles **71**-**75**.

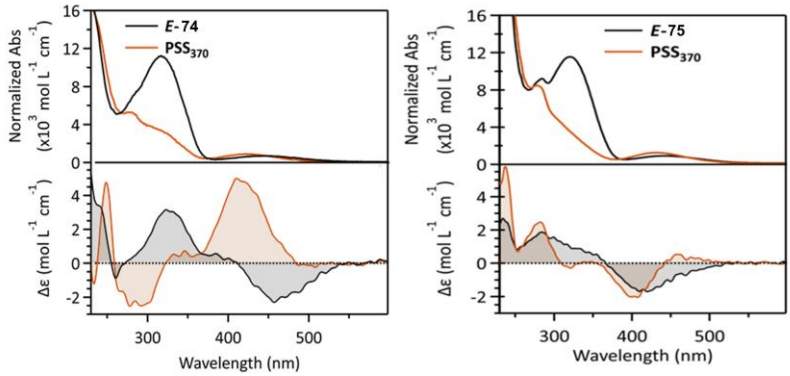


**Figure 28** Normalized absorption and circular dichroism spectra of **74** (11.4 μM) and **75** (65 μM) in *E*-isomer (black line) or at $PSS_{370}$ (orange line) in MeCN. Adapted from Ref. 31 with permission from The Royal Society of Chemistry.

## 4 Conclusion and Outlook

Up to 38-membered photosensitive carbohydrate-based macrocycles have been developed since 2006. Although only a limited number has been reported (18 fluorescent and 14 photochromic), these photoresponsive glycomacrocycles have shown diverse interesting properties. Main applications for the fluorescent glycomacrocycles concerned the fluorescent sensing for heavy metal ions like $Cu^{2+}$ and $Hg^{2+}$, and DNA intercalation, where the recognition roles played by the carbohydrate moiety have been clearly demonstrated. Photoswitchable glycomacrocyclic compounds have showed excellent photowitching properties, with high photo- and thermo-stability, opening the window for various applications in chemistry, supramolecular chemistry and material sciences. Reversible switching of conformation, shape, and solubility can be achieved by repetitive UV/vis illumination. Chiroptical properties have been observed for D-glucose-linked cyclic dithiophene polymer and azobenzene-functionalized glycomacrocycles, and circularly polarized luminescence properties for chiral polycyclothiophenes. Furthermore, the *o*-azobenzene-embedded glycomacrolactones have been successfully employed as photoresponsive chiral dopants for cholesteric liquid crystals able to perform mechanical work. One of them is able to generate photo-, thermo- and mechano-responsive organogel. Considering the diversity and numerous applications of glycomacrocycles described to date[10] and the potential of the photosensitive systems,[1-9] there is plenty of room for the further development of photoresponsive glycomacrocyclic compounds by incorporating different fluorophores and molecular photoswitches or both of them for analytical and biomedical applications, for photopharmacology, for organic synthesis by designing photoswitchable catalysis, or as smart functional materials, and so on.

## List of abbreviation :

| | |
|---|---|
| BODIPY | Boron difluoride dipyrromethene |
| CD | Circular dichroism |
| CLC | Cholesteric liquid crystals |
| CPL | Circularly polarized luminescence |
| CuAAC | Cu(I)-catalyzed azido-alkyne cycloaddition |
| DFT | Density-functional theory |
| DNA | Deoxyribonucleic acid |
| EB | Ethidium bromide |
| HPLC | High performance liquid chromatography |
| HTP | Helical twisting power |
| NIS | *N*-iodosuccinimide |
| PL | Photoluminescence |
| PSS | Photostationary state |
| SAC | Sugar-aza-crown |
| TD-DFT | Time-dependent density functional theory |
| TfOH | Triflic acid |

## References

[a]*Université Paris-Saclay, ENS Paris-Saclay, CNRS, Photophysique et Photochimie Supramoléculaires et Macromoléculaires, Institut d'Alembert, 4 avenue des sciences, 91190 Gif-sur-Yvette, France. Tel: 33 0181875603; E-mail: joanne.xie@ens-paris-saclay.fr*

Footenotes: This review paper is dedicated to the memory of Prof. Gérard Descotes.


1 W. Xu, Z. Zeng, J.-H. Jiang, Y.-T. Chang and Lin Yuan, *Angew. Chem. Int. Ed*., 2016, **55**, 13658.

2 J. Zhang, X. Chai, X.-P. He, H.-J. Kim, J. Yoon and H. Tian, *Chem. Soc. Rev*., 2019, **48**, 683.

3 Kyle P. Carter, Alexandra M. Young, and Amy E. Palmer, *Chem. Rev*., 2014, **114**, 4564.

4 Z. L. Pianowski, *Chem. Eur. J.*, 2019, **25**, 5128.

5 W.-C. Xu, S. Sun, and S. Wu, *Angew. Chem. Int. Ed*., 2019, **58**, 9712.

6 D.-H. Qu, Q.-C. Wang, Q.-W. Zhang, X. Ma and He Tian, *Chem. Rev*., 2015, **115**, 7543.

7 R. Göstl, A. Senf and S. Hecht, *Chem. Soc. Rev.*, 2014, **43**, 1982.

8 R. Dorel and B. L. Feringa, *Chem. Commun.*, 2019, **55**, 6477.

9 K. Hull, J. Morstein and D. Trauner, *Chem. Rev*., 2018, **118**, 10710.

10 J. Xie and N. Bogliotti, *Chem. Rev*., 2014, **114**, 7678.

11 J. K. M. Ågren, J. F. Billing, H. E. Grundberg and U. J. Nilsson, *Synthesis*, 2006, **18**, 3141.

12 J. Xie, M. Ménand, S. Maisonneuve and R. Métivier, *J. Org. Chem.*, 2007, **72**, 5980.

13 M. Ménand, J.-C. Blais, L. Hamon, J.-M. Valéry and J. Xie, *J. Org. Chem.*, 2005, **70**, 4423.

14 M. Ménand, J.-C. Blais, J.-M. Valéry and J. Xie, *J. Org. Chem.*, 2006, **71**, 3295.

15 A. Bordes, A. Poveda, T. Troadec, A. Franconetti, A. Ardá, F. Perrin, M. Ménand, M. Sollogoub, J. Guillard, J. Désiré, R. Tripier, J. Jiménez-Barbero and Y. Blériot, *Org. Lett.*, 2020, **22**, 2344.

16 A. Bordes, A. Poveda, N. Fontelle, A. Ardá, J. Guillard, Y. B. Ruan, J. Marrot, S. Imaeda, A. Kato, J. Désiré, J. Xie, J. Jiménez-Barbero and Y. Blériot, *Carbohydr. Res.*, 2021, **501**, 108258.

17 Y.-C. Hsieh, J.-L. Chir, H.-H. Wu, P.-S. Chang and A.-T. Wu, *Carbohydr. Res.*, 2009, **344**, 2236.

18 Y.-C. Hsieh, J.-L. Chir, S.-T. Yang, S.-J. Chen, C.-H. Hu and A.-T. Wu, *Carbohydr. Res.*, 2011, **346**, 978.

19 Y.-C. Hsieh, J.-L. Chir, H.-H. Wu, C.-Q. Guo and A.-T. Wu, *Tetrahedron Lett.*, 2010, **51**, 109.

20 Y.-C. Hsieh, J.-L. Chir, W. Zou, H.-H. Wu and A.-T. Wu, *Carbohydr. Res.*, 2009, **344**, 1020.

21 I. Ling, R. Hashim and K. J. Sabah, *RSC Adv*., 2015, **5**, 88038.

22 Y. Yu, N. Bogliotti, J. Tang, J. Xie, *Eur. J. Org. Chem.*, 2013, 7749.

23 S. Chen, R. Zhang, X. Wang, R. Yu, M. Li, S. Ren and T. Jiang, *Carbohydr. Res.*, 2016, **429**, 48.

24 T. Ikai, K. Takayama, Y. Wada, S. Minami, C. Apiboon and K.-i. Shinohara, *Chem. Sci*., 2019, **10**, 4890.
25 T. Ikai, S. Minami, S. Awata, S. Shimizu, T. Yoshida, M. Okubo and K.-i. Shinohara, *Polym. Chem*., 2018, **9**, 5504.
26 F. Fournier, C. Afonso, M. Ménand, L. Hamon, J. Xie and J.-C. Tabet, *Eur. J. Mass Spectr.*, 2008, **14**, 61.
27 G. Despras, J. Hain and S. O. Jaeschke, *Chem. Eur. J*., 2017, **23**, 10838.
28 C. Lin, S. Maisonneuve, R. Métivier and J. Xie, *Chem. Eur. J*., 2017, **23**, 14996.
29 J. Hain and G. Despras, *Chem. Commun.*, 2018, **54**, 8563.
30 C. Lin, S. Maisonneuve, C. Theulier and J. Xie, *Eur. J. Org. Chem*., 2019, 1770.
31 C. Lin, J. Jiao, S. Maisonneuve, J. Mallétroit and J. Xie, *Chem. Commun*. 2020, **56**, 3261.
32 Y. Kim, N. Mafy, S. Maisonneuve, C. Lin, N. Tamaoki and J. Xie, *ACS Appl. Mater. Interfaces*, 2020, **12**, 52146.
33 H. M. D. Bandarab and S. C. Burdette, *Chem. Soc. Rev*., 2012, **41**, 1809.